

CHEMISTRY 
A EUROPEAN JOURNAL

Supporting Information

© Copyright Wiley-VCH Verlag GmbH & Co. KGaA, 69451 Weinheim, 2007

A Spectroscopic Study of the Reduction of Geometrically-restrained Viologens

Andrew C. Benniston*, Anthony Harriman, Peiyi Li, James P. Rostron, Ross W.
Harrington and William Clegg

*[a] Molecular Photonics Laboratory & Crystallography Laboratory, School of Natural Sciences,
University of Newcastle, Newcastle upon Tyne, NE1 7RU, United Kingdom*

CONTENTS

Table S1. Calculated parameters from the X-ray structure determinations.

Table S2. Summary of crystallographic experimental data.

Figure S1. Absorption spectrum recorded for the monocation radical derived from methyl viologen.

The radical was generated by spectroelectrochemical techniques in deoxygenated acetonitrile solution containing background electrolyte.

Figure S2. Energy-level diagram proposed for the monocation radical, showing the various absorption transitions.

Figure S3. EPR spectrum (blue trace) recorded for the monocation radical derived from methyl viologen by electrochemical reduction in deoxygenated acetonitrile solution. The lower panel (red trace) shows the simulated EPR spectrum, based on the hyperfine coupling constants given in the text.

Figure S4. Molecular formulae drawn for the diquat and phenanthroline series of electron acceptors mentioned in the text. The right-hand panel shows dependence of the first reduction potential on the computed dihedral angle.

Figure S5. Normalized plots showing the effect of dihedral angle on the heat of formation (blue curve) and energy of the LUMO (red curve) for the monocation radical derived from methyl viologen.

Figure S6 Cyclic voltammograms obtained for all the compounds investigated. Data were recorded at room temperature in acetonitrile containing 0.1 M TBAB as supporting electrolyte.

Figure S7. Absorption spectra recorded for the various monocation radicals in deoxygenated acetonitrile solution, using spectroelectrochemical techniques. The spectrum shown for C4 refers to a relatively high concentration and is intended to depict the effects of aggregation. Here, the dashed curve refers to a 20-fold diluted sample.

Figure S8. The computed structures and partial atomic charges for the monocation radicals derived from methyl viologen and **C2**.

Table S1. Calculated parameters from the X-ray structure determinations.

| Compound | $f / ^\circ$ ^(a) | $R_{CC} / \text{\AA}$ | $R_{OO} / \text{\AA}$ ^(b) | $R_{HH} / \text{\AA}$ ^(c) | N ^(d) |
|------------|-----------------------------|-----------------------|--------------------------------------|--------------------------------------|--------------------|
| C1 | 12.2 | 1.498(3) | 2.329 | 1.80 | 3 |
| C2 | 54.3 | 1.491(5) | 2.830 | 2.65 | 4 |
| C3 | 55.8 | 1.495(9) | 2.829 | 2.77 | 5 |
| C4 | 61.3 | 1.489(3) | 2.968 | 2.85 | 6 |
| CE5 | 57.7 | 1.511(9) | 2.753 | 2.43 | 13 |

(a) Torsion angle C–C–C–C about the inter-ring bond involving the ortho-C atoms attached to O atoms. (b) Distance between the alkoxy O atoms. (c) Distance between the two ortho H atoms of the pyridinium rings; for this calculation, the C–H distances have been extended to the expected internuclear separation of 1.08 Å. (d) Number of bridging atoms in the tether. NB For $MV^{2+}Cl_2$, R_{CC} is 1.464 Å.

Table S2. Summary of crystallographic experimental data.

| | C1 | C2 | C3 | C4 | CE5 |
|----------------------------|---|---|---|---|---|
| formula | $C_{13}H_{14}N_2O_2^{2+} \cdot 2PF_6^-$ | $C_{14}H_{16}N_2O_2^{2+} \cdot 2PF_6^-$ | $C_{15}H_{18}N_2O_2^{2+} \cdot 2PF_6^-$ | $C_{16}H_{20}N_2O_2^{2+} \cdot 2PF_6^-$ | $C_{20}H_{28}N_2O_5^{2+} \cdot 2PF_6^-$ |
| M_r | 520.2 | 534.2 | 548.3 | 562.3 | 666.4 |
| crystal description | colorless block | colorless block | colorless block | colorless slab | colorless rod |
| crystal dimensions [mm] | $0.42 \times 0.24 \times 0.20$ | $0.42 \times 0.24 \times 0.22$ | $0.42 \times 0.28 \times 0.18$ | $0.42 \times 0.38 \times 0.22$ | $0.10 \times 0.05 \times 0.05$ |
| crystal system | monoclinic | monoclinic | monoclinic | monoclinic | orthorhombic |
| space group | <i>P2/n</i> | <i>C2/c</i> | <i>C2/c</i> | <i>C2/c</i> | <i>Pna2₁</i> |
| <i>a</i> [Å] | 15.1107(19) | 19.2472(13) | 18.756(4) | 19.327(4) | 37.042(11) |
| <i>b</i> [Å] | 6.1141(7) | 8.8968(6) | 8.9762(18) | 8.9564(18) | 8.746(3) |
| <i>c</i> [Å] | 21.9360(16) | 11.5035(8) | 12.383(3) | 12.869(3) | 8.111(2) |
| β [°] | 109.487(9) | 100.682(1) | 103.45(3) | 105.59(3) | |
| <i>V</i> [Å ³] | 1910.5(4) | 1935.7(2) | 2027.6(8) | 2145.7(8) | 2627.9(13) |
| <i>Z</i> | 4 | 4 | 4 | 4 | 4 |
| <i>T</i> [K] | 150 | 150 | 150 | 150 | 120 |
| μ [mm ⁻¹] | 0.356 | 0.354 | 0.340 | 0.324 | 0.287 |
| data collected | 13645 | 8254 | 14000 | 12864 | 16899 |
| unique data | 3289 | 2348 | 1325 | 2459 | 5308 |

| | | | | | |
|--|-------------|-------------|-------------|-------------|-------------|
| R_{int} | 0.0433 | 0.0225 | 0.0512 | 0.0646 | 0.0688 |
| refined parameters | 505 | 146 | 160 | 156 | 393 |
| $R (F, F^2 > 2\sigma)$ | 0.0341 | 0.0570 | 0.0563 | 0.0410 | 0.0965 |
| $R_w (F^2, \text{all data})$ | 0.0862 | 0.1097 | 0.1605 | 0.1178 | 0.2585 |
| goodness of fit (all F^2) | 1.038 | 1.291 | 1.117 | 1.053 | 1.097 |
| difference map extremes [e Å ⁻³] | 0.23, -0.29 | 0.44, -0.38 | 0.78, -0.37 | 0.49, -0.33 | 1.03, -0.52 |

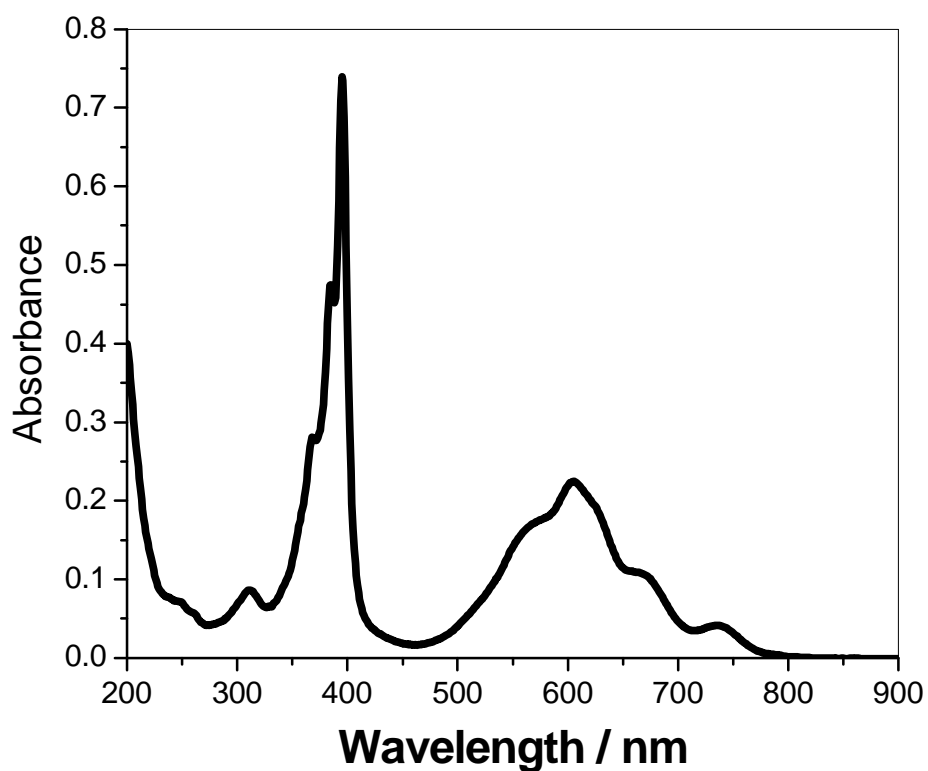


Figure S1. Absorption spectrum recorded for the monocation radical derived from methyl viologen. The radical was generated by spectroelectrochemical techniques in deoxygenated acetonitrile solution containing background electrolyte.

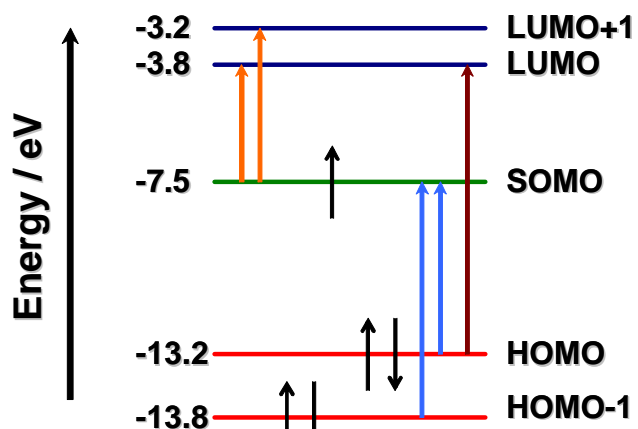


Figure S2. Energy-level diagram proposed for the monocation radical, showing the various absorption transitions.

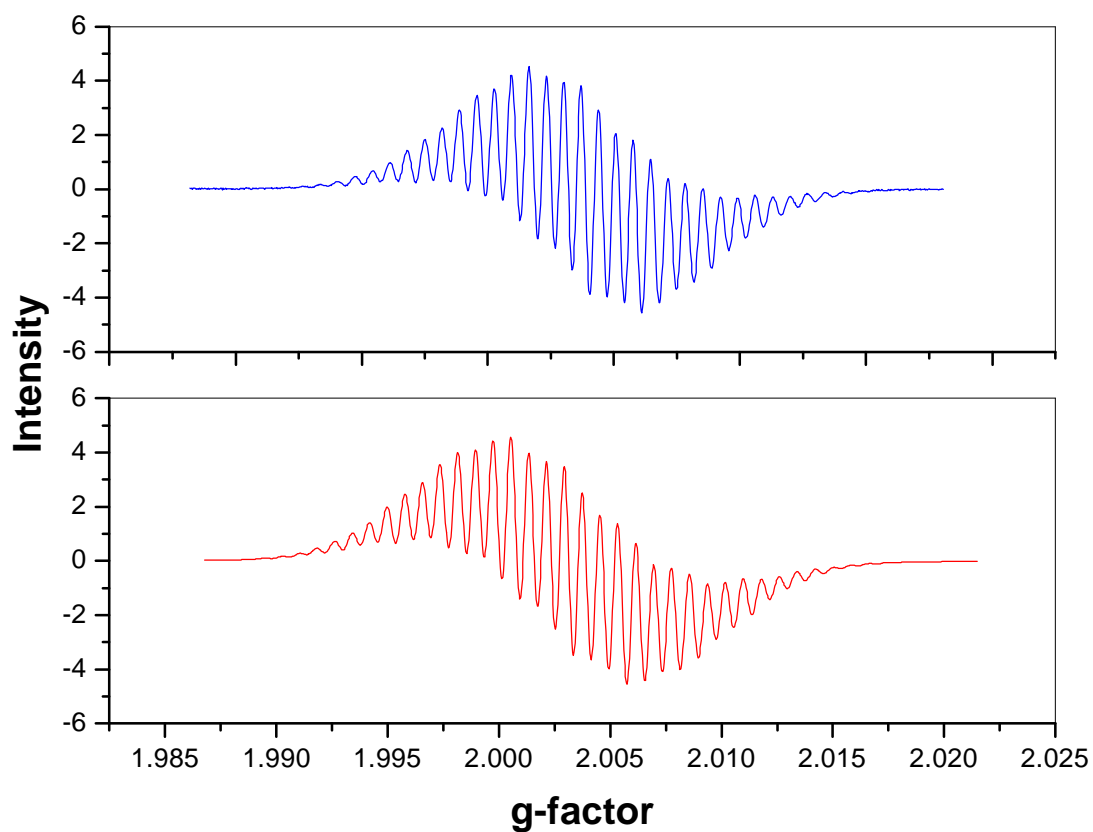
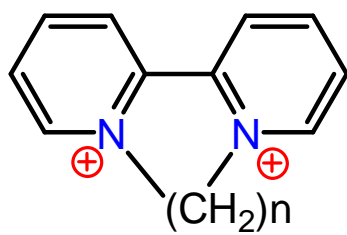
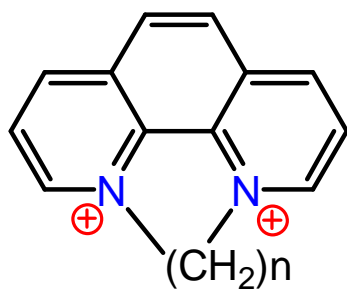


Figure S3. EPR spectrum (blue trace) recorded for the monocation radical derived from methyl viologen by electrochemical reduction in deoxygenated acetonitrile solution. The lower panel (red trace) shows the simulated EPR spectrum, based on the hyperfine coupling constants given in the text.



n=2,3 or 4



n=2 or 3

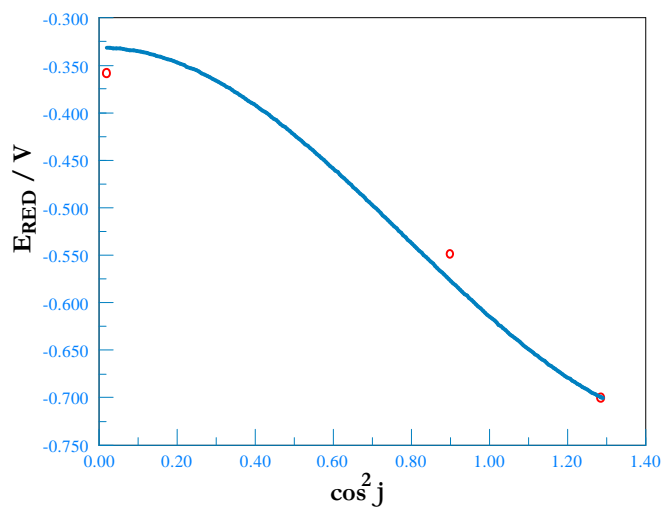


Figure S4. Molecular formulae drawn for the diquat and phenanthroline series of electron acceptors mentioned in the text. The right-hand panel shows dependence of the first reduction potential on the computed dihedral angle.

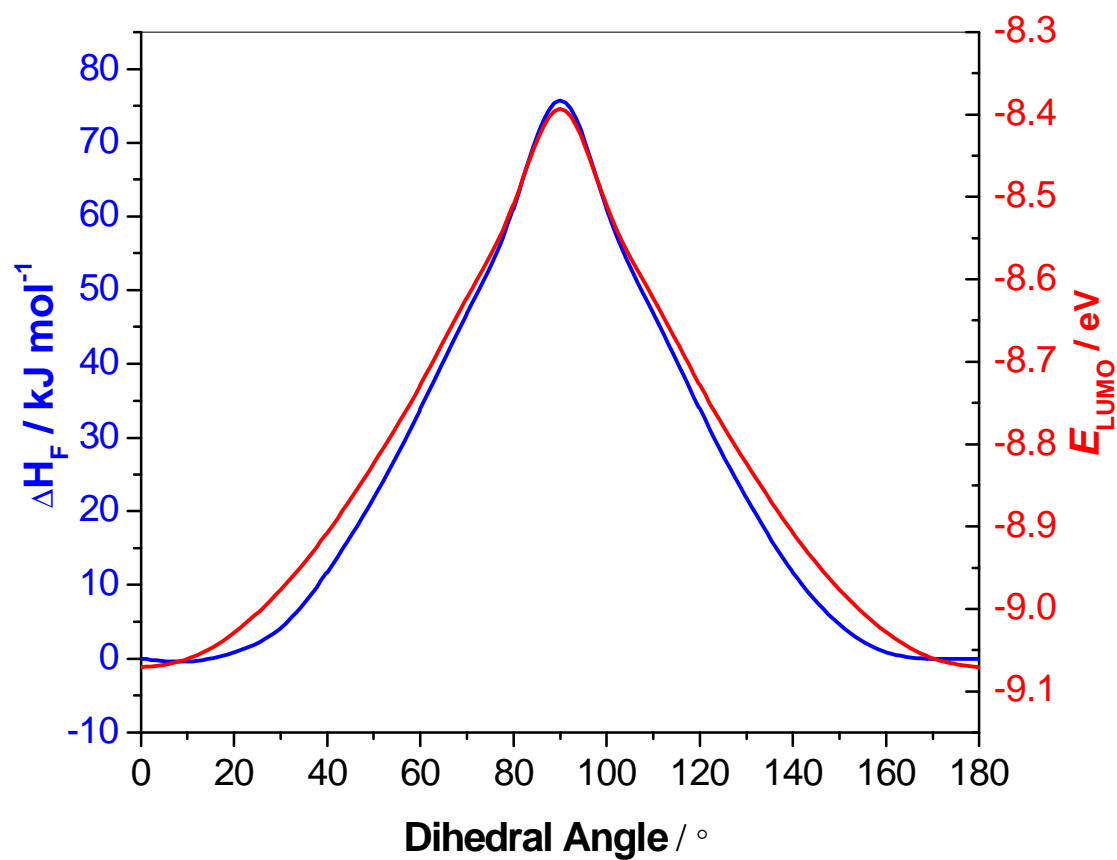


Figure S5. Normalized plots showing the effect of dihedral angle on the heat of formation (blue curve) and energy of the LUMO (red curve) for the monocation radical derived from methyl viologen.

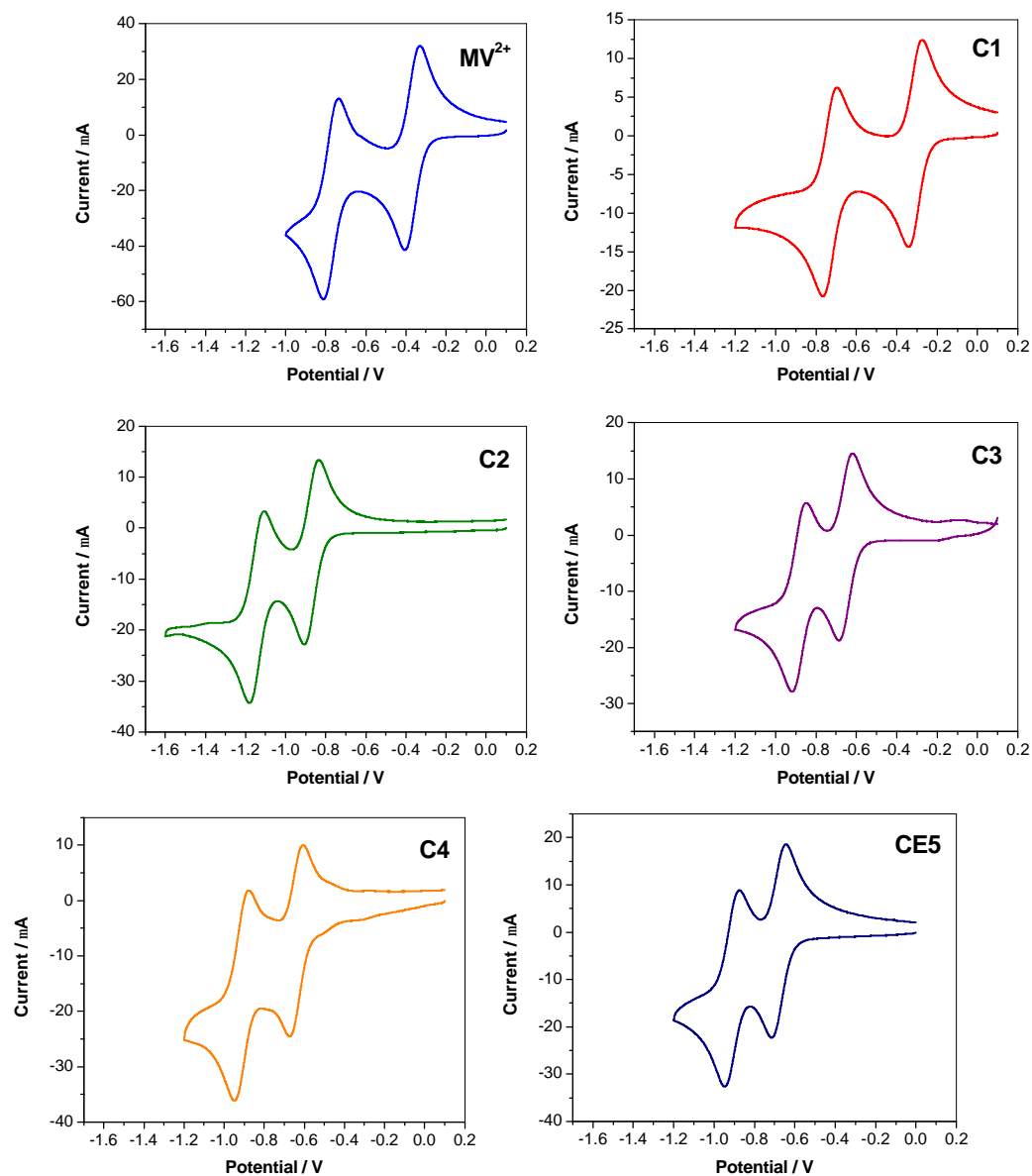


Figure S6 Cyclic voltammograms obtained for all the compounds investigated. Data were recorded at room temperature in acetonitrile containing 0.1 M TBAB as supporting electrolyte.

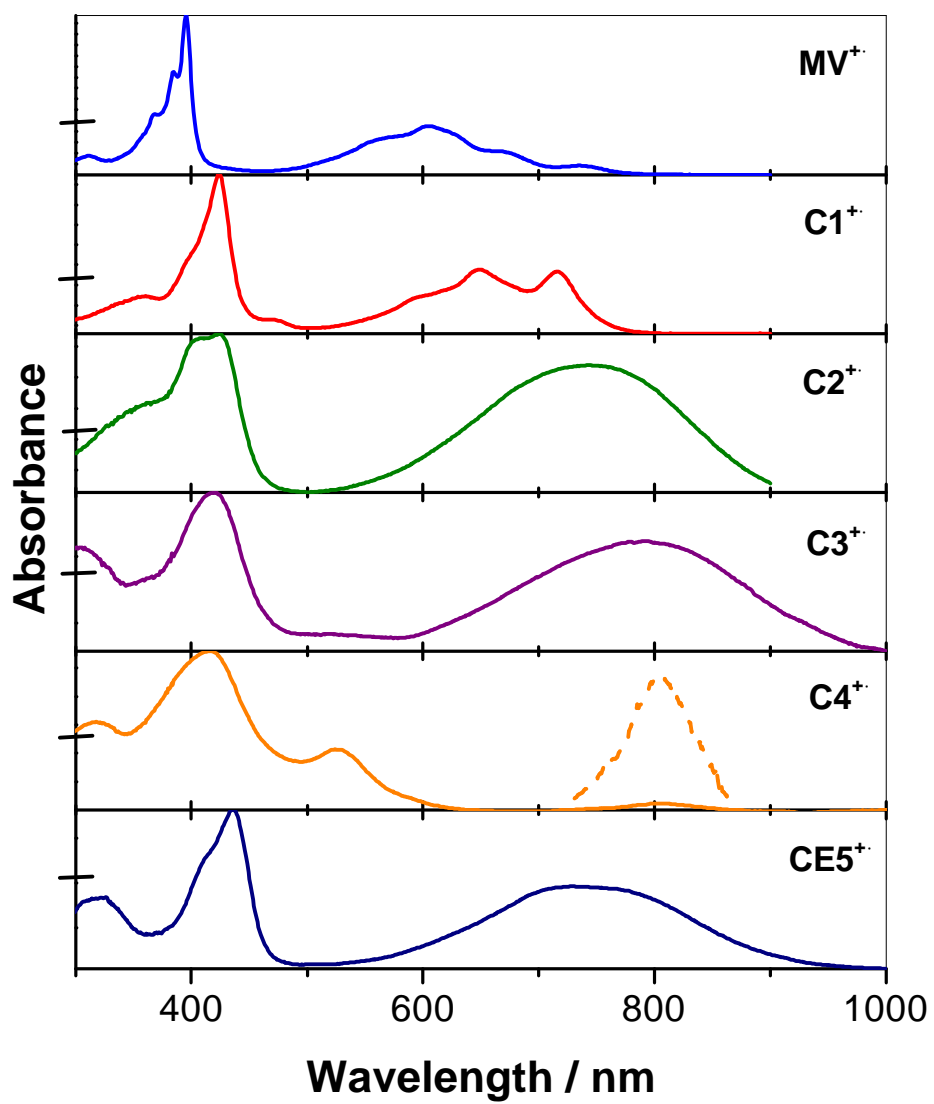


Figure S7. Absorption spectra recorded for the various monocation radicals in deoxygenated acetonitrile solution, using spectroelectrochemical techniques. The spectrum shown for C4 refers to a relatively high concentration and is intended to depict the effects of aggregation. Here, the dashed curve refers to a 20-fold diluted sample.

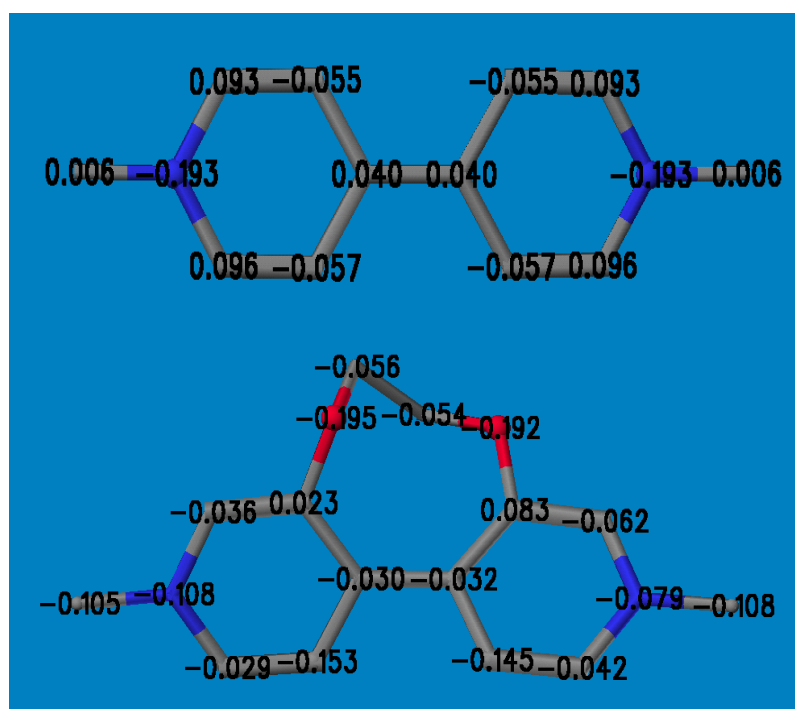


Figure S8. The computed structures and partial atomic charges for the monocation radicals derived from methyl viologen and **C2**.

